Proceedings of *The Riddle of Cooling Flows in Galaxies and Clusters of Galaxies*: E16
May 31 – June 4, 2003, Charlottesville, Virginia, USA
Ed. T. H. Reiprich, J. C. Kempner, & N. Soker

Ni Abundance in the Core of the Perseus Cluster: An Answer to the Significance of Resonant Scattering

Fabio Gastaldello[1,2] and Silvano Molendi[1]

[1] *IASF - CNR, via Bassini 15, I-20133 Milano, Italy*
[2] *University of Milano Bicocca, Dip. di Fisica, P.za della Scienza 3 I-20133 Milano, Italy*

Using an *XMM-Newton* observation of the Perseus cluster we show that the excess in the flux of the 7–8 keV line complex previously detected by *ASCA* and *BeppoSAX* is due to an overabundance of Nickel rather than to an anomalously high Fe Heβ/Fe Heα ratio. This observational fact leads to the main result that resonant scattering, which was assumed to be responsible for the supposed anomalous Fe Heβ/Fe Heα ratio, is no longer required. The absence of resonant scattering points towards the presence of significant gas motions (either turbulent or laminar) in the core of the Perseus cluster. The presence of the well-known Fe abundance gradient is confirmed, while the presence of a Ni abundance gradient, which would add another piece of evidence to the scenario of a central enhancement of SNIa ejecta in cD clusters, is complicated by the complex thermal structure of the gas.

1. Introduction

The X-ray emission from clusters is due to a diffuse, tenuous (with typical densities of 10^{-4}–$10^{-2}\,\mathrm{cm}^{-3}$), and hot (with typical temperatures of 10^{7}–$10^{8}\,\mathrm{K}$) thermal plasma. Although for these ranges of density and temperature the gas is optically thin to Thomson scattering for the continuum, it can be optically thick in the resonance X-ray lines of highly ionized atoms of heavy elements (Gilfanov et al. 1987). Apart from other interesting observable effects (Sazonov et al. 2002), the major effect of resonance scattering (the absorption of a line photon followed by immediate re-emission) is to distort the surface-brightness profile of the cluster in the resonance line due to diffusion of photons from the dense core into the outer regions of the cluster. This must be taken into account when attempting to determine element abundances from X-ray spectroscopic observations of galaxy clusters. In fact only with the key assumption that the plasma is optically thin line equivalent widths can unambiguously convert to element abundances, when fitting CCD spectra with the available plasma codes. In presence of resonant scattering the true abundances in the core of clusters are significantly underestimated because the line emission is attenuated due to photons scattered out of the line of sight. To make things worse, the most promising line for resonant scattering is the Heα Fe emission line at 6.7 keV (Gilfanov et al. 1987; Sazonov et al. 2002) which is also one of the most prominent emission line in cluster spectra and in general drives the global abundance determination.

High sensitivity and high resolution spectrometers are needed to directly measure the spectral features of resonant scattering (as modification of the line profile or resolution of the He-like line into its constituents in order to determine directly the effects of scattering) and polarimeters, to detect the polarized scattered radiation (Costa et al. 2001; Sazonov et al. 2002). Currently the simplest method to reveal and estimate the presence of resonance scattering is to compare the fluxes of an expected optically thick line and of an optically thin one and to check if it is correctly modeled by a plasma code assuming optically thin emission. This was done in the past with *ASCA* and *BeppoSAX* for the ratio between Heα Fe line at 6.7 keV and the Heβ Fe line at 7.90 keV (which is expected to have an optical depth typically smaller than one for resonant scattering) and in particular the best data were the ones for the Perseus cluster.

Molendi et al. (1998) analyzed data collected with the MECS on board *BeppoSAX* and found that the ratio of the flux of the 7–8 keV line complex to the 6.7 keV line was significantly larger than predicted by optically thin plasma code and that the ratio decreases with increasing cluster radius. They noted that this effect could be explained either by resonant scattering or by a Ni overabundance, eventually favoring the former explanation. On the contrary Dupke & Arnaud (2001), according to the experimental evidence of a central enhancement of SNIa ejecta in cD clusters, favored the over-abundant Ni explanation.

These were the two hypothesis that the resolution and sensitivity of past instruments could not resolve. *XMM-Newton* has now for the first time the combination of resolution and effective area at high energies to give an unambiguous answer to the question. Our aim is to try to solve this controversy. In Section 2 we give information about the *XMM-Newton* observation and data preparation. In Section 3 we present spatially resolved measurements of temperature and Ni and Fe abundances. In Section 4 we discuss our results and draw our conclusions.

At the nominal redshift of Perseus (z=0.0183), $1'$ corresponds to 22.2 kpc ($H_0 = 70$ km s^{-1} Mpc^{-1}, $\Omega_\mathrm{m} = 1 - \Omega_\Lambda = 0.3$). In the following analysis, all the quoted errors are at 1σ (68.3 per cent level of confidence) unless stated otherwise.

2. **Observation and Data Preparation**

The Perseus cluster was observed with *XMM-Newton* (Jansen et al. 2001) during Revolution 210, with the THIN1 filter and in Full Frame Mode, for 53.6 ks for MOS and 51.2 ks for PN, but resulting in an effective exposure time (as written in the keyword LIVETIME of the fits event file) of 53.1 ks for the MOS and 24.7 ks for the PN. The observation was badly affected by a significantly enhanced background level due to soft protons. For details on the observation and background level see Churazov et al. (2003) and Gastaldello & Molendi (2003). Using standard soft proton cleaning criteria all the observation would be rejected. Our approach was therefore to consider all the observation for two reasons: we can exploit the fact that Perseus is the brightest X-ray cluster and it is so bright in its central zone that the background, also in presence of a high level of soft protons as we have in our observation, is not important; moreover we can try to model the soft proton which contaminate the spectra using in first approximation a power law as a background model (which means that the model is not convolved via the effective area of the instrument). The self-consistency and viability of our approach will be shown in the results.

We generated calibrated event files using the publicly available SASv5.3.3. We have accumulated spectra in 9 concentric annular regions centered on the emission peak with bounding radii $0.'5$–$1'$, $1'$–$2'$, $2'$–$3'$, $3'$–$4'$, $4'$–$5'$, $5'$–$6'$, $6'$–$8'$, $8'$–$10'$, $10'$–$14'$. We did not consider the inner bin inside $0.'5$ in order to avoid contamination by the power law spectrum of the Seyfert cD galaxy NGC 1275. Spectra have been accumulated for the three cameras independently and the blank fields provided by the calibration teams were used as background (Lumb 2002). Background spectra have been accumulated from the same sky regions as the source spectra, after reprojection onto the sky attitude of the source (this ensures the proper subtraction in the same way as it was performed in detector co-ordinates, see Lumb 2002).

The vignetting correction has been applied to the effective area generating effective area files for the different annular regions using the SAS task *arfgen*. We generate flux weighted arf using exposure corrected images of the source as detector maps and the parameter *extended source* switched to true, following the prescription of Saxton & Siddiqui (2002). Spectral results for the cluster A3528 obtained in this way and with the vignetting correction applied directly to the spectra (Arnaud et al. 2001) are practically the same (Gastaldello et al. 2003). We also correct the PN spectra for out of time events following the prescriptions of Grupe (2001). The redistribution matrices used are m1_r6_all_15.rmf (MOS1), m2_r6_all_15.rmf (MOS2) and, depending on the mean "RAWY" of the region, the set of ten single-pixel matrices, from epn_ff20_sY0.rmf to epn_ff20_sY9.rmf, and double-pixel matrices, from epn_ff20_dY0.rmf to epn_ff20_dY9.rmf, for PN.

Due to its higher effective area (further increased by the use of doubles data) and similar spectral resolution at high energies, the PN camera will be the leading instrument in our analysis and the one for which the results are most compelling, in particular for what concerns the Ni abundance. There are still some problems for what concern the three EPIC cameras cross-calibration and in particular at high energies the study of power-law sources returns harder spectra for MOS1, intermediate for MOS2 and then the softest for PN (Kirsch et al. 2002). Also our analysis of the galaxy cluster A3528 gives systematically higher temperatures and abundances for MOS1 with respect to MOS2 and PN. The conclusions of a recent work aimed at assessing the EPIC spectral calibration using a simultaneous *XMM-Newton* and *BeppoSAX* observation of 3C273 strengthen this fact: the MOS-PN cross calibration has been achieved to the available statistical level except for the MOS1 in the 3–10 keV band which returns flatter spectral slope (Molendi & Sembay 2003).

3. **Results**

3.1. *Spectral Modeling and Energy Ranges Used*

All spectral fitting has been performed using version 11.2.0 of the XSPEC package (Arnaud 1996).

As a first step we concentrate on the hard band which is the one of interest to determine the abundances of iron and nickel and also to make a direct comparison with the MECS results. We use three different energy bands: 3–10 keV, 3–7 keV in order to have a band less contaminated by the hard tail of soft protons, and the 3–13.5 keV and 3–12 keV for PN and MOS respectively in order to have more data to acceptably model the soft protons background. When fitting the first two bands we analyze the spectra with a single temperature VMEKAL model (Mewe et al. 1985; Kaastra 1992; Liedahl et al. 1995) with the multiplicative component WABS to account for the Galactic absorption fixed at the value of $0.143 \times 10^{22}\,\mathrm{cm}^{-2}$ (according to Schmidt et al. 2002). We leave the abundances of Ar, Ca, Fe and Ni (the only elements which have emission lines in the range 3–10 keV) free and keep all the other abundances fixed to half the solar values (Fukazawa et al. 2000). When fitting the wider high energy band, more contaminated by soft protons, we add a power law background model (VMEKAL+POW/B in XSPEC) in order to model the soft proton background component.

As a second step we fit the entire energy band 0.5–10 keV with two models: (i) a single temperature model leaving N_{H} to vary freely (the fit is substantially improved with respect to the one with N_{H} fixed to the Galactic value) and the abundance of O, Ne, Mg, Si, S, Ar, Ca, Fe and Ni. For the outer annuli, when required from the previous analysis in the hard band, we add the pow/b component with normalization and slope fixed at the best fit values found; (ii) a two temperature model (WABS*(VMEKAL+VMEKAL) in XSPEC) where the metal abundance of each element of the second thermal component is bound to be equal to the same parameter of the first thermal component. As for the single temperature model we add the pow/b component when required. The two temperature model is a rough attempt to reproduce the complex spectrum resulting from pro-

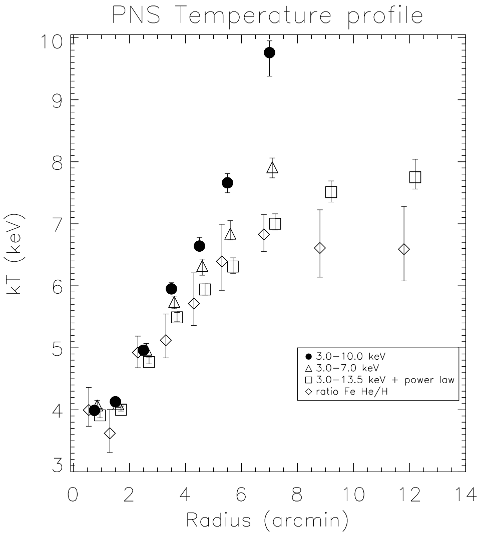

FIG. 1.— PN singles temperature profile. Uncertainties are at the 68% level for one interesting parameter ($\Delta\chi^2 = 1$). Full circles represent the temperature obtained using the range 3–10 keV, open triangles the temperature obtained using the range 3–7 keV and open squares the temperature obtained by using the range 3–13.5 keV and adding to the source model a power law background component. In the last two bins we do not show the temperatures obtained in the 3–10 keV and 3–7 keV bands because they are larger than 10 keV. Diamonds represent the temperature obtained by the ratio of the fluxes of Heα to Hα Fe lines.

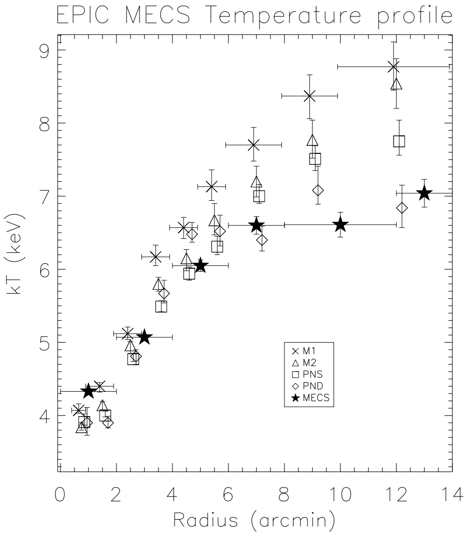

FIG. 2.— Temperature profiles obtained with the various EPIC cameras compared with the temperature profile obtained with the MECS instrument on board *BeppoSAX*. Crosses represent temperatures obtained with MOS1, open triangles with MOS2, open squares with PN singles, open diamonds with PN doubles and full stars with the MECS.

jection effects, azimuthal mean of very different emission regions (like holes and luminous regions in the Perseus cluster, see Schmidt et al. 2002; Fabian et al. 2002) and an atmosphere probably containing components at different temperatures, as in M87 (Kaiser 2003; Molendi 2002).

We also allow the redshift to be a free parameter in order to account for any residual gain calibration problem. We adopt for the solar abundances the values of Grevesse & Sauval (1998), where Fe/H is 3.16 $\times$ 10^{-5}. To make comparison with previous measurements, a simple rescaling can be made to obtain the values with the set of abundances of Anders & Grevesse (1989), where the solar Fe abundance relative to H is 4.68 $\times$ 10^{-5} by number.

3.2. *1T Results in the High Energy Band*

In Fig. 1 we show the temperature profile obtained analyzing the single events spectrum for the PN camera. This is also an example of our working procedure. The full circles refer to the results obtained using the 3–10 keV band, while the open triangles indicates the results obtained using the 3–7 keV band with the Ni abundance frozen to the best fit value obtained in the 3–10 keV band. It is clear that where the source is overwhelmingly bright the hard component of the soft proton does not affect the spectrum and there are no differences between the temperatures obtained in different energy bands, while in the outskirts of the cluster, where the source brightness is lower and the soft protons become important, the fitted plasma temperature reaches incorrect and unphysically high values and large residuals at high energy are present. With the open squares we show the temperature obtained by fitting not only the source but also the soft protons with a power law background model, in the energy band 3–13.5 keV: as we expect in the inner region adding the background component does not affect the temperature determination nor statistically improve the fit, on the contrary in the outer regions the temperature are significantly reduced and the fit is improved, eliminating the residuals at high energies. For example in the $6'$–$8'$ ring the simple single temperature fit gives a χ^2 of 1502 for 1137 degrees of freedom, while the fit with the power law background model in addition gives a χ^2 of 1258 for 1288 d.o.f.

To confirm our results we compare the temperatures obtained in this way with those obtained with the MECS instrument on board *BeppoSAX* (De Grandi & Molendi 2002a).

The temperature profiles, shown in Fig. 2, are in good agreement at least up to $8'$, apart from the differences in the three cameras due to the cross-calibration problems we discussed before (confirmed also with the superb statistics of Perseus). In the outer rings between 8 and $14'$ the increasing importance of background relative to source counts prevent us from recovering a correct temperature with our method (see De Grandi & Molendi 2002a, for a more general discussion about *XMM-Newton* and *BeppoSAX* temperature determinations and the greater sensitivity of the latter over the former to low surface brightness regions due to much lower background).

With a determination of the temperature structure we can address the issue of metal abundances measure and attempt to discriminate between the presence of resonant scattering or the supersolar abundance of Nickel. Resonant scattering is increasingly important towards the

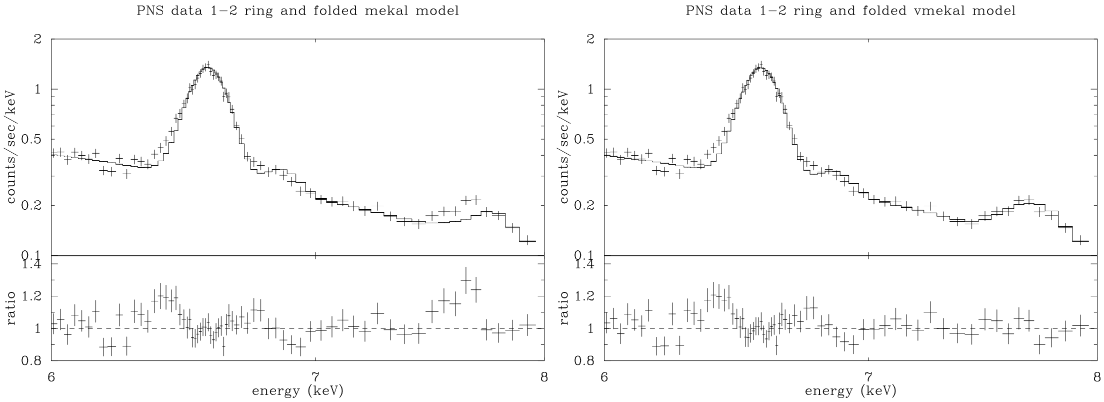

FIG. 3.— PN singles data for the $1'$–$2'$ bin in the 6–8 keV band and the corresponding fit with a MEKAL model, on the left, and with a VMEKAL model, on the right, together with the corresponding ratios of data with respect to models.

center of the cluster so we choose our two inner bins to test its presence. Fitting the spectra with a MEKAL model, assuming solar ratios, actually does not reproduce the 8 keV line complex. As shown in the left panel of Fig. 3 for the $1'$–$2'$ bin, the emission is underestimated as for previous missions (see Fig. 1 of Molendi et al. 1998 for example). However the data show for the first time that the excess is due to an incorrect modeling of the Ni Heα line complex at 7.75–7.80 keV (in the rest frame of the source) and not to an underestimation of the Fe Heβ line which is correctly modeled. In fact if we fit the data with a VMEKAL model, we eliminate almost completely the residuals and give a better fit with a Ni abundance of 1.23 in solar units, as shown in the right panel of Fig. 3. The fit with a MEKAL model gives a χ^2 of 855 for 802 d.o.f for the $0\farcm5$–$1'$ bin and 1116 for 1023 d.o.f. for the $1'$–$2'$ bin, while a fit with a VMEKAL model (with Ar and Ca fixed to 0.5 $Z/Z_\odot$, because they are not important in driving the fit, in order to have only the Ni abundance as additional free parameter) gives a χ^2 of 835 for 801 d.o.f. for the first bin and 1092 for 1022 d.o.f. for the second bin, with $\Delta\chi^2$ which are statistically significant at more that the 99.9% according to the F-test (the value of the F statistics is F=19.2 with a probability of exceeding F of 1.4×10^{-5} for the first bin and F=22.5 with a probability of exceeding F of 2×10^{-6} for the second bin).

We can conclude that the ratio of Heβ/Heα Fe lines is not anomalously high with respect to the optically thin model and that it is not necessary to invoke resonant scattering in the core of the Perseus cluster. The excess in the flux in the 8 keV line complex with respect to a MEKAL model is entirely due to Ni overabundance with respect to solar values, as was previously suggested (Dupke & Arnaud 2001).

The reader will notice some residuals in the Heα Fe line complex at 6.7 keV. This is an instrumental artifact present only in the inner bins out to $2'$ of the PN camera we suspect connected to some residual CTI problems due to the high flux of the Perseus cluster. The net effect is to lower the energy resolution broadening the line profile. We test that this does not affect our results fitting spectra for our two inner bins with a bremsstrahlung model plus two Gaussians fixed at the energies of the Fe Heα at 6.67 keV and Fe Heβ at 7.90 keV leaving the redshift, width and normalizations of the two lines as free parameters. We find that the Gaussian widths of the Heα lines in the two bins are 5.3×10^{-2} keV in the $0\farcm5$–$1'$ bin and 4.5×10^{-2} keV in the $1'$–$2'$ bin. If we force the Heβ to have up to a width of 8×10^{-2} the excess due to the Ni Heα line blend at 7.75–7.80 keV is still significantly present. This instrumental effect is evident because of the large equivalent width of the Fe line at 6.67 keV and does not alter significantly the measure of metal abundances as we show further on.

We can make some other important considerations investigating another line ratio, namely the Heα Fe line complex at 6.7 keV over the Hα Fe line at 6.97 keV. This ratio allows a robust and independent determination of the temperature, because as the temperature increases the contribution from the He Fe line decreases while the contribution from the H Fe line increases. Thus the intensity ratio of the two lines can be used to estimate the temperature. This was done in the past determining the variation with the temperature of the centroid of the blend of the two lines, because gas proportional counters did not have sufficient spectral resolution to resolve the two lines (Molendi et al. 1999). Now with *XMM-Newton* we can resolve the lines, measure separately their intensity and use their ratio as a thermometer. To do that we obtain a calibration curve of the line flux ratio as a function of temperature simulating spectra with MEKAL model and the PN singles response matrix with a step size of 0.1 keV, fixing the metal abundance of 0.3 solar units and the normalization to unity in XSPEC units (however the flux ratio is independent of these two quantities), with an exposure time of 100 ks to ensure negligible statistical errors. We then model the spectra with a bremsstrahlung model plus two Gaussians for the two iron lines, in the energy range 3–10 keV and obtaining the fluxes of the two lines from the best fit models. We obtain a calibration curve identical to that of Nevalainen et al. (2003). We then measure the line flux ratio from the cluster PN singles data using the energy range 5.0–7.2 keV to minimize the dependence from the continuum and calibration accuracy and to better describe the lines. We fitted each spectrum with a bremsstrahlung model

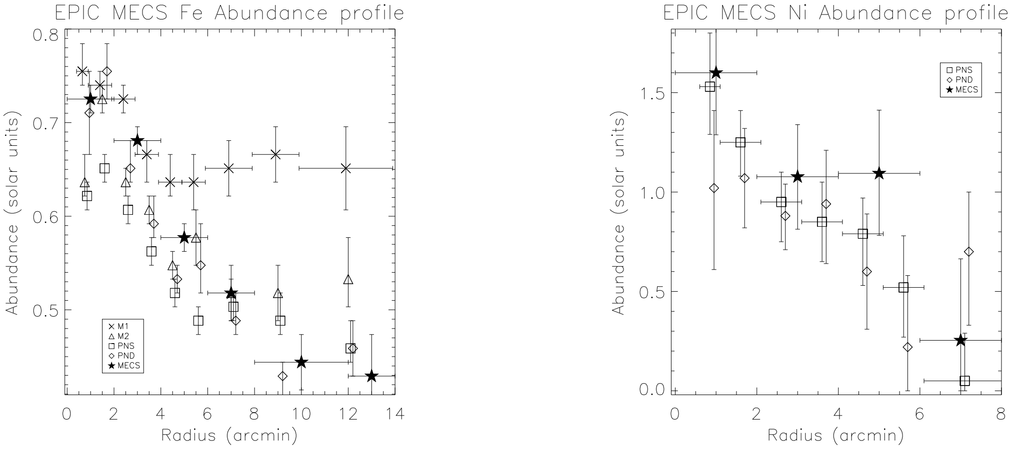

Fig. 4.— Abundance profiles for Fe, on the top, and for Ni, on the bottom, obtained with the various EPIC cameras compared with the abundance profiles obtained with the MECS instrument on board *BeppoSAX*. As in Fig. 2, crosses refers to MOS1, open triangles to MOS2, open squares to PN singles, open diamonds to PN doubles and full stars to MECS.

plus two Gaussians (using ZBREMSS plus two ZGAUSS models in XSPEC) leaving all the parameters free, including the redshift (to take into account any possible gain calibration problem), except the line energies. The fits for all the annular bins were good with a reduced χ^2 never worse than 1.1 and the results for the temperature derived from line flux ratio are plotted as diamonds in Fig. 1.

As we can see also this independent temperature determination is in good agreement with all the others at least out to $3'$ where the cluster is very bright and in good agreement out to $8'$ with the measurement obtained from the model with the power law background component, confirming the validity of our modeling. In the last two bins the temperature derived from the line ratios agrees well with the MECS measurement and starts to differ from the determination with power law background component, pointing to the fact that our modeling is not sufficient to fully take into account the background in these bins where the source is too dim compared to the soft proton background. We can conclude that our temperature determination is reliable out to $8'$.

The concordance between line ratio and continuum temperature determinations adds another piece of evidence against resonant scattering. In fact since the Fe Hα line optical depth is 1.8 times smaller than the Fe Heα one (this is the difference in their oscillator strength), if resonant scattering is present, we would expect the ratio of Heα/Hα lines to be lower than in the optically thin case. In turn this would lead to an overestimate of the temperature. Since this is not the case we can conclude that resonant scattering is not present.

In Fig. 4 we plot the abundance profiles of Fe and Ni determined by our best fit model (thermal model plus power law component for the soft proton background, in the 3–13.5 keV band for PN and 3–12 keV for MOS). We find an evident gradient in both elements: for Fe it agrees well with previous determinations, as the *BeppoSAX* one (without considering the corrections for resonant scattering, as done in Molendi et al. 1998), while we have for the first time a detailed abundance gradient for Ni, with measurements reliable out to $8'$ (we show only the PN data as we discussed before). We stop at this radius because at larger radii the temperature determination is no longer reliable and strong emission lines of Ni, Cu and Zn induced by particle events affect the spectrum in the crucial range 7.5–8.5 keV (Freyberg et al. 2002). It is evident that there are some problems with the iron determination by MOS1, as we also found in A3528.

Knowing that the excess in the 8 keV line complex is due to the Ni line, we can go back to BeppoSAX-MECS data and fit them with a VMEKAL model allowing Ni abundance to be free. We find an abundance profile in agreement with the more detailed *XMM-Newton* one, as shown in Fig. 4.

3.3. *1T and 2T Results in the 0.5–10 keV Band*

We fit one and two temperature models to MOS2 and PN single data (we avoid MOS1 data for the calibration problems explained in the previous section) in the full energy band 0.5–10 keV. Single temperature models cannot adequately fit the entire band spectra, giving temperatures systematically lower than the ones obtained in the hard band and leaving large residuals at high energies. These facts hint towards the presence of more than one temperature component, in-fact a two temperature model yields a substantially better fit than the one temperature model, although it is still not statistically acceptable.

The temperature profiles for PN singles data and MOS2 are shown in Fig. 5: the two temperature fit shows the presence of a hot and of a cold component. The temperature of the hot component especially in the outer bins matches the temperature determined with the fit in the hard band, while the temperature of the cold component is less constrained, being about 2 keV in the PN fit and oscillating between 2 and 3 keV in the MOS2 fit. The relative normalization of the two components, shown in Fig. 6, shows that the cool component is stronger in the center of the cluster, as we expect for cool core clusters.

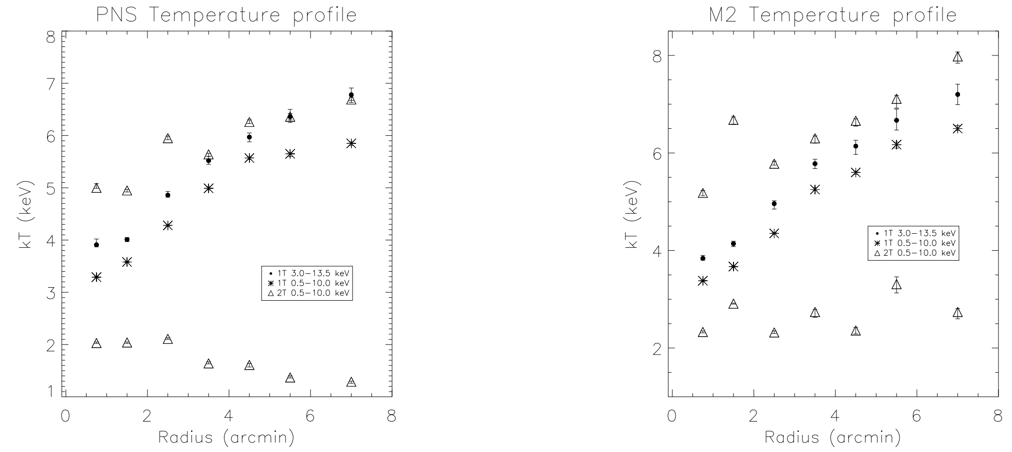

FIG. 5.— Temperature profiles obtained in the entire 0.5–10 keV band using one temperature (crosses) and two temperature models (open triangles, both the temperatures of the hot and cold component are shown) and, for comparison, the one obtained with the best fit model in the hard band (full circles), for PN singles data, on the top, and for MOS2 data, on the bottom.

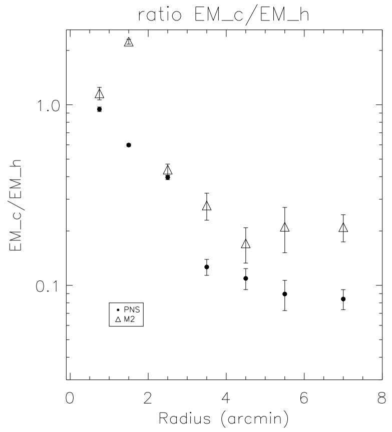

FIG. 6.— Ratio of the normalizations of the two temperature components, obtained by a two temperature model fitted in the 0.5–10 keV band, for PN single data (full circles) and MOS2 data (open triangles).

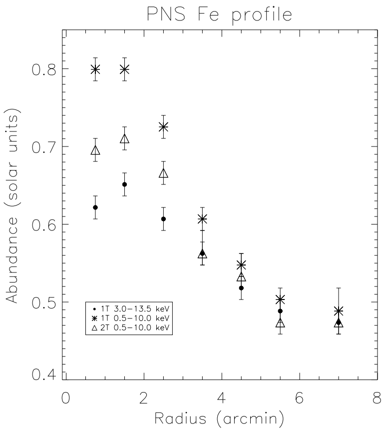

FIG. 7.— Fe abundance profiles obtained in the entire 0.5–10 keV band using one temperature (crosses) and two temperature models (open triangles) and, for comparison, the one obtained with the best fit model in the hard band (full circles), for PN singles data.

Although there are some puzzling results, as in the inner two bins of the MOS2 data where the fitting procedure prefers to give more importance to the cool component, and the presence of cool emission also in the outer bins where the emission should be negligible (although the cooling radius for Perseus is $\sim 6'$, Peres et al. 1998).

The Fe abundance profile, shown in Fig 7 (only PN values are shown, the M2 values being practically the same) is not substantially changed and in particular the abundance gradient is even more evident. Instead for the Ni abundance profile, shown in Fig 8, the evidence for a gradient is not present. In fact adding a linear component improves the fit ($\chi^2 = 1.9$ for 5 d.o.f) with respect to a constant ($\chi^2 = 1.9$ for 6 d.o.f) for the PN Ni abundances derived by the 1T model in the hard band, while the Ni profile derived by the 2T model in the entire band is essentially flat (fitting a constant returns a $\chi^2 = 3$ for 6 d.o.f and a linear component does not improve the fit, $\chi^2 = 2.9$ for 6 d.o.f). We caution the reader that the 2T modelization is rather complex, because some not completely justified assumptions are made, as for example that the abundances of the two components are equal, and there is some degeneracy in the contribution of the two X-ray emission components and the soft proton power-law background (see for MOS2 and PN the substantial difference in the temperature of the cool component[1]). Therefore the derived Ni abundance should be taken with some caution. Moreover it is very difficult to explain, in presence of a confirmed Fe abundance gradient, a flat Ni abundance profile and a Ni/Fe ratio which increases going outward.

---

[1] With the latest release of SAS, version 5.4.1, which revise the quantum efficiency for the MOS and the PN, the agreement between the two detectors should be better, in particular in the low energy band.

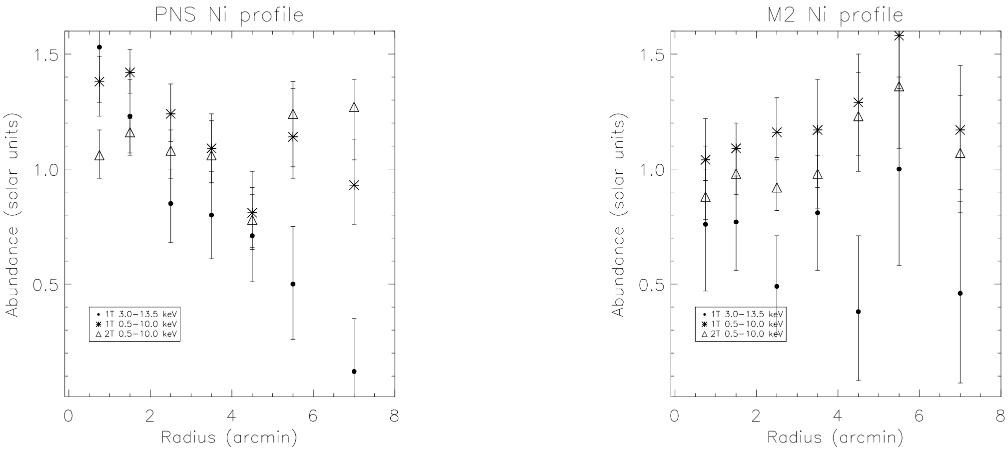

FIG. 8.— Ni abundance profiles obtained in the entire 0.5–10 keV band using one temperature (crosses) and two temperature models (open triangles) and, for comparison, the one obtained with the best fit model in the hard band (full circles), for PN singles data, on the top, and for MOS2 data, on the bottom.

4. **Discussion**

Our main result can be summarized as follows: there is no need to invoke resonant scattering in the Fe Heα line in the Perseus cluster core and the Fe abundance determination with optically thin emission models is reliable.

Resonant scattering should be important in the core of galaxy clusters, this is particularly true for the Fe Heα line in the core of the Perseus cluster (it has an optical depth of 3.3 according to Sazonov et al. 2002). The optical depth of a resonance line depends on the characteristic velocities of small scale internal motions, which could seriously diminish the depth τ (Gilfanov et al. 1987, see Mathews et al. 2001 for an example of a detailed calculation in presence of turbulent motions). The absence of a clear evidence of resonant scattering strongly points towards the presence of significant gas motions. In fact, following Gilfanov et al. (1987), the optical depth is

$$\tau = \tau^0 \left(1 + v_{turb}^2 / v_{Fe}^2\right)^{-1/2}, \tag{1}$$

where τ^0 is the optical depth at the line center in the absence of turbulence (in spectroscopy the word turbulence is used for all hydrodynamic motions of unknown pattern which cause a broadening of the spectral lines. In hydrodynamics turbulence has a much more restricted meaning), v_{turb} is the turbulent velocity of the gas and $v_{Fe} = (2kT_e/M_{Fe})^{1/2} \sim c_s/8.8$ is the thermal speed of the iron ions and c_s denotes the adiabatic sound speed in the ICM. Thus the absence of resonant scattering, $\tau < 1$, and assuming $\tau^0 = 3.3$ (Sazonov et al. 2002), implies gas motions with characteristic velocities greater than $0.36\,c_s$, i.e a Mach number $M \gtrsim 0.36$.

Studies of optical line emission in the central regions of ellipticals reveal chaotic gas kinematics typically about 0.2–0.4 of the sound speed in the hot gas (Caon et al. 2000) and since small, optically visible line-emitting regions at T $\sim 10^4$ K are likely to be strongly coupled to the ambient gas, as some models predict (Sparks et al. 1989) and clear correlation between Hα+[N II] and X-ray luminosities suggests, the hot gas should share the same turbulent velocities. The first clear example of resonant scattering, acting on the $2p-3d$ line of Fe XVII at 15.0 Å (0.83 keV), has been recently found in the giant elliptical galaxy NGC 4636 (Xu et al. 2002) using the reflection grating on board *XMM-Newton* and measuring the cross dispersion profile of the ratio between an optically thin emission blend, the two $2p-3s$ lines of Fe XVII at 17.0-17.1 Å (0.73 keV) and the optically thick line at 15.0 Å. Xu et al. (2002) found that if an average turbulent velocity dispersion more than 1/10 of the sound speed is added to the assumed Maxwellian the model becomes incompatible with the ratio of the 17.1 Å/15.0 Å lines. We remind that the detection of the resonant scattering is only in the inner $1'$, in-fact the phenomenon does not affect spectra extracted within a full-width of $2'$ (Xu et al. 2002). Another elliptical, NGC 5044, was observed with the RGS (Tamura et al. 2003) and no evidence of resonant scattering was found in spectra extracted in the full $2'$. If also in this case a cross dispersion analysis where to show resonant scattering, these would rule out possible associations at least at these inner scales with optically line-emitting gas, because NGC 4636 and NGC 5044 are the most striking examples of chaotic gas kinematics in the sample of Caon et al. (2000).

Another possible source of gas motions is the activity of an AGN, which is now thought to be widespread in the core of galaxy clusters and strongly related to hot bubbles, for which one of the best cases is indeed the Perseus cluster (Fabian et al. 2002). The induced motions could be either turbulent or laminar, as suggested by the recent *Chandra* and optical results in Fabian et al. (2003a,b) (see the discussion about the flow causing the horseshoe Hα filament and the derived velocity of 700 km s^{-1} which for a sound speed of about 1170 km s^{-1}, for a temperature of 5 keV, implies $M \sim 0.6$ or about the sound waves generated by the continuous blowing of bubbles). AGN activity could explain the lack of resonant scattering also in the other best candidate M87 (but see also the discussion suggesting caution for this interpretation in the analysis of RGS data for M87 of Sakelliou

et al. 2002).
What is becoming progressively clearer is that resonant scattering effects must be small and confined on small inner scales.

The Fe abundance gradient confirms the general picture of an increase of SNIa ejecta in the center of relaxed cD clusters. The determination of the Ni abundance profile is important, because Ni is almost exclusively produced by SNIa and the presence of a gradient also in this element could be a crucial confirmation of this general picture (see De Grandi & Molendi 2002b which report measures of Fe and Ni for a sample of 22 clusters observed with *BeppoSAX* and in particular their Fig. 6 showing a segregation between relaxed cD clusters and not relaxed clusters, with the former with greater Fe and Ni abundances with respect to the latter). The Ni abundance gradient is evident in the fit in the high energy band and, looking back at the *BeppoSAX* data, we can attribute the excess in the 8 keV line complex to an increased Ni abundance. However the complex thermal structure of the gas prevents us from reaching a robust determination of the Ni abundance profile. Detailed temperature and abundances maps are required to address this issue.

This work is based on observations obtained with *XMM-Newton*, an ESA science mission with instruments and contributions directly funded by ESA Member States and the USA (NASA).

References

Anders, E. & Grevesse, N. 1989, Geochimica et Cosmochimica Acta, 53, 197

Arnaud, K.A., 1996, Astronomical Data Analysis Software and Systems V, eds. Jacoby G. and Barnes J., p17, ASP Conf. Series volume 101

Arnaud, M., Neumann, D. M., Aghanim, N., Gastaud, R., Majerowicz, S., Hughes, J. P. 2001, A&A, 365, L80

Caon, N., Macchetto, d., Pastoriza, M., 2000, ApJS, 127, 39

Churazov, E., Forman, W., Jones, C., Boöringer, H., 2003, ApJ, 590, 225

Costa, E., Soffitta, P., Bellazzini, R., Brez, A., Lumb, N., Spandre, G., 2001, Nature, 411, 662

De Grandi, S. & Molendi, S., 2002a, ApJ, 567, 163

De Grandi, S. & Molendi, S., 2002b, in Chemical Enrichment of Intracluster and Intergalactic Medium, ASP Conference Proceedings Edited by Roberto Fusco-Femiano and Francesca Matteucci. Vol 253, p.3

Dupke, R. A. & Arnaud, K.A., 2001, ApJ, 548, 141

Fabian, A.C., Celotti, A., Blundell, K.M., Kassim, N.E., Perley, R.A., 2002, MNRAS, 331, 369

Fabian, A.C., Sanders, J.S., Allen, S.W., Crawford, C.S., Iwasawa, K., Johnstone, R.M., Schmidt, R.W., Taylor, G.B., 2003a, MNRAS in press, (astro-ph/030636)

Fabian, A.C., Sanders, J.S., Crawford, C.S., Conselice, C.J., Gallagher III, J.S., Wyse, R.F.G., 2003b, MNRAS in press, (astro-ph/030639)

Finoguenov, A., Matsushita, K., Böhringer, H., Ikebe, Y., Arnaud, M., 2002, A&A, 381, 21

Freyberg, M.J., Briel, U.G., Dennerl, K., Haberl, F., Hartner, G., Kendziorra, E., Kirsch, M., 2002, in Symp. New visions of the X-ray Universe in the XMM-Newton and Chandra era (ESA SP-488; Noordwijk: ESA)

Fukazawa, Y., Makishima, K., Tamura, T., Nakazawa, K., Ezawa, H., Ikebe, Y., Kikuchi, K., Ohashi, T., 2000, MNRAS, 313, 21

Gastaldello, F. & Molendi, S., 2002, ApJ, 572, 160

Gastaldello, F., Ettori, S., Molendi, S., Bardelli, S., Venturi, T., Zucca, E., 2003a, A&A in press, (astro-ph/0307342)

Gastaldello, F. & Molendi, S., 2003b, ApJ in press, (astro-ph/0309582)

Gilfanov, M.R., Sunyaev,R.A., Churazov, E.M., 1987, Sov. Astron. Lett., 13, 3

Grupe, D., 2001, http://wave.xray.mpe.mpg.de/xmm/cookbook/EPIC_PN/ootevents.html

Grevesse, N. & Sauval, A. J., 1998, Space Science Reviews, 85, 161

Jansen, F., Lumb, D., Altieri, B., Clavel, J., Ehle, M., Erd, C., Gabriel, C., Guainazzi, M., Gondoin, P., Much, R., Munoz, R., Santos, M., Schartel, N., Texier, D., Vacanti, G. 2001, A&A, 365, L1

Kaastra, J.S., 1992, An X-ray Spectral code for Optically Thin Plasmas (Internal SRON-Leiden Report, updated version 2.0)

Kaiser, C.R., 2003, MNRAS in press, (astro-ph/0305104)

Kirsch, M. et al., "Status of the EPIC calibration and data analysis", 2002, XMM-SOC-CAL-TN-018

Liedahl, D. A., Osterheld A. L., Goldstein, W. H. 1995, ApJ, 438, L115

Lumb, D., "EPIC background files", 2002, XMM-SOC-CAL-TN-016

Marty, P.B., Kneib, J.P., Sadat, R., Ebeling, H., Smail, I., 2002, proceedings SPIE vol. 4851 (astro-ph/0209270)

Mathews, W.G., Buote, D.A., Brighenti, F., 20001, ApJ, 550, L31

Matsushita, K., Belsole, E., Finoguenov, A., Böhringer, H., 2002, A&A, 386, 77

Mewe, R., Gronenschild, E. H. B. M., van den Oord, G. H. J., 1985, A&AS, 62, 197

Molendi, S., Matt, G., Antonelli, L.A., Fiore, F., Fusco-Femiano, R., Kaastra, J., Maccarone, C., Perola, C., 1998, ApJ, 499, 618

Molendi, S., De Grandi, S., Fusco-Femiano, R., Colafrancesco, S., Fiore, F., Nesci, R., Tamburelli, F., 1999, ApJ, 525, L73

Molendi, S., 2002, ApJ, 580, 815

Molendi, S. & Sembay, S., 2003, XMM-SOC-CAL-TN-0036

Nevalainen, J., Lieu, R., Bonamente, M., Lumb, D., 2003, ApJ, 584, 716

Nomoto, K., Iwamoto, K., Nakasato, N., Thielemann, F. K., Brachwitz, F., Tsujimoto, T., Kubo, Y., Kishimoto, N. 1997, Nucl.Phys. A, 621, 467

Peres, C.B., Fabian, A.C., Edge, A.C., Allen, S.W., Johnstone, R.M., White, D.A., 1998, MNRAS, 298, 416

Pratt, G.W. & Arnaud, M., 2002, A&A, 394, 375

Sakelliou, I., Peterson, J.R., Tamura, T., Paerels, F.B.S., Kaastra, J.S., Belsole, E., Böhringer, H., Branduardi-Raymont, G., Ferrigno, C., den Herder, J.W., Kennea, J., Mushotzky, R.F., Vestrand, W.T., Worrall, D.M., 2002, A&A, 391, 903

Saxton, R.D. & Siddiqui, H., "The status of the SAS spectral response generation tasks for XMM-EPIC", 2002, XMM-SOC-PS-TN-43

Sazonov, S.Yu., Churazov, E.M., Sunyaev, R.A., 2002, MNRAS, 333, 191

Schmidt, R.W., Fabian, A.C., Sanders, J.S., 2002, MNRAS, 337, 71

Smith, R. K., Brickhouse, N. S., Liedahl, D. A., Raymond, J. C. 2001, ApJ, 556, L91

Sparks, W.B., Macchetto, D., Golombeck, D., 1989, ApJ, 345, 153

Tamura, T., Kaastra, J.S., Makishima, K., Takahashi, I., 2003, A&A, 399, 407

Xu, H., Kahn, S.M., Peterson, J.R., Behar, E., Paerels, F.B.S., Mushotzky, R.F., Jernigan, J.G., Brinkman, A.C., Makishima, K., 2002, ApJ, 579, 600